Electronic Supplementary Material (ESI) for ChemComm.

Electronic Supplementary Information for

Selective quantification of nanoplastics in environmental matrices by asymmetric flow field – flow fractionation with total organic carbon detection

Marfua Mowla[a*], Sheyda Shakiba[a], and Stacey M. Louie[a*†]

[a]Department of Civil and Environmental Engineering, University of Houston, Houston, TX, USA, 77204

[*]Equal contribution

[†]Corresponding author:

Email: slouie@central.uh.edu

Phone: 1-713-743-8646

Pages: 30

Figures: 11

Tables: 2

Table of Contents

S1. Materials and sample preparation

S1.1. Polystyrene (PS) nanoplastics

PS nanoplastics were purchased at a nominal concentration of 1 wt % PS (10 g L^{-1}) with 0.1 wt % Tween 20 surfactant (1 g L^{-1}) and 2 mM sodium azide preservative. Four sizes were obtained with nominal diameters of 50 nm, 100 nm, 200 nm, and 500 nm (and manufacturer-reported actual diameters of 41 ± 7 nm, 124 ± 17 nm, 220 ± 49 nm, and 541 ± 144 nm). The nanoplastics were bath sonicated (CPXH 2800, Branson Ultrasonic Corporation, Brookfield, CT, USA) for 30 to 40 s immediately prior to use. For sample preparation, the stocks were either diluted to 500 mg L^{-1} in deionized water (DIW) for each of the four PS sizes, or prepared as a mixture containing 500 mg L^{-1} of each PS sizes from 10 gL^{-1} stock. The diluted mixture stock was further diluted in DIW to mixtures containing 5 mg L^{-1}, 10 mg L^{-1}, 15 mg L^{-1} and 20 mg L^{-1} of all four PS sizes as calibration standards for the asymmetric flow field – flow fractionation (AF4) analyses. For all other samples except where indicated otherwise, the individual PS sizes and mixtures were evaluated using 20 mg L^{-1} of each size of nanoplastics.

A gravimetric analysis was used to verify the mass concentrations of the PS stocks. 1 mL of PS stock of each size was added into pre-weighed 20 mL glass vials (which were pre-treated in a furnace at 550 °C for 2 h, then cooled to room temperature) and lyophilized for 48 hours at 0.2 mbar and -80 °C (FreeZone Freeze Dry system, Labconco Corporation, Kansas City, MO, USA). The dry mass of material was recorded; results are reported in Section S6.

S1.2. Tween 20 (polysorbate 20)

The PS stocks as purchased included Tween 20 (i.e., polysorbate 20). Pure Tween 20 was purchased (VWR International, Radnor, PA, USA) to prepare known samples for analysis on the total organic carbon (TOC) analyzer in order to correct measurements on the PS nanoplastics for the Tween 20 contribution. The pure Tween 20 was serially diluted to ≈ 20 g L^{-1} and 500 mg L^{-1} with DIW (with exact concentrations determined gravimetrically), and finally diluted to 10 mg L^{-1} as C for batch TOC measurements.

S1.3. Kaolin clay

Hydrous aluminum silicate (kaolin clay) was acquired from BASF (ASP 600, BASF Corporation, Charlotte, NC, USA) with reported mean size of 0.6 μm. This ASP 600 material was previously recommended to serve as the clay portion of simulated sediments.[1-3] Following prior methods for preparation,[1] the clay was first treated to remove any combustible organic matter as follows. A 40 mL glass vial was first treated in a furnace (Lindberg Blue M, Thermo Scientific, Waltham, MA, USA) for 550 °C for 2 h. Then, 10 g of clay was weighed into the vial and treated for 550 °C for 1 h. The mass loss of the clay was ≈ 3.9 wt %. The treated clay was then used to prepare a 1 g L^{-1} suspension in a 50 mL centrifuge tube (VWR International, Radnor, PA, USA), first by adding 2 mL of DIW to the 35 mg of clay and bath sonicating for 3 minutes to wet the clay, then adding 13 mL of DIW and probe sonicating the suspension (Fisherbrand Model 120 Sonic Dismembrator, Fisher Scientific, Hampton, NH, USA) for 15 minutes at 100% amplitude, 80% pulse cycle (8 s on, 2 s off) to disperse the clay. Note that 15 mL is the recommended maximum sample volume for the ultrasonication probe used. The remaining 20 mL of DIW was added after the probe sonication. The stock suspension was purified of large particles by centrifuging at 800 rpm (74.41g) for 9.5 min in a fixed angle rotor (R_{min} = 6.94 cm, R_{max} = 10.4 cm, F15-8x50cy rotor, Sorvall Legend XTR centrifuge, ThermoFisher Scientific, Hampton, NH, USA); this time was calculated to sediment particles larger than ≈ 1 μm, assuming spherical particles with density 2.65 g cm^{-3}, as in prior research to process soil slurries for AF4 analyses.[4] The supernatant containing the clay colloids was collected and used for all further experiments and analyses, and the pH was measured to be 5.91. The pelleted clay in the centrifuge tube was lyophilized at 0.2 mbar and -80 °C for 24 h to determine the mass of clay removed and compute the remaining concentration of clay colloids in the supernatant as 570 mg L^{-1}.

S1.4. Elliott soil humic acid (ESHA)

ESHA (Standard V, Catalog # 5S102H) was purchased from the International Humic Substances Society (IHSS) and used to represent background dissolved organic matter that can be present in environmental samples. A soil humic acid was selected over aquatic natural organic matter for its higher molecular weight, which presents a greater challenge for separation from nanoplastics considering that a higher proportion of the ESHA will be retained in the AF4 analysis (using a 10 kDa ultrafiltration membrane as the accumulation wall). A stock solution of 2 g L^{-1} of ESHA was prepared in DIW, adjusted to pH 7 with 1 M NaOH and 0.1 M HCl, and allowed to dissolve for 24 h on an end-over-end rotator at 25 rpm. The stock was then filtered using a 0.22 µm polyethersulfone (PES) syringe filter (EMD Millipore, Burlington, MA, USA) and stored at 4 °C for further use. The concentrations (as carbon) of the unfiltered and filtered stocks were 925 mg_C L^{-1} and 780 mg_C L^{-1}, respectively, as determined by batch TOC analysis (Section S2.3).

S1.5. Nile Red

Nile Red dye (99%, pure, Acros Organics, Fair Lawn, NJ, USA) was prepared at 1 g L^{-1} in methanol (ultrapure HPLC grade, Alfa Aesar, Ward Hill, MA, USA), bath sonicated to dissolve, and kept in the dark at 4 °C for further use. For fluorescent labeling, samples were spiked with 10 mg L^{-1} of Nile Red directly from the 1 g L^{-1} stock.

S2. Instrumentation and methods

S2.1. Batch dynamic light scattering (DLS) and electrophoretic light scattering (ELS)

Batch DLS and ELS measurements were collected on the PS nanoplastics and clay colloids on a Zetasizer Nano ZS instrument (Malvern Instruments, Westborough, MA, USA). For both measurements, samples were equilibrated at 25 °C in the instrument compartment for 2 min, and five measurement replicates per sample were collected and averaged. For DLS, cumulants analysis was applied to obtain *z*-average sizes. For ELS, samples were loaded into a disposable folded capillary cell (DTS1070, Malvern Instruments, Westborough, MA, USA). The automatic voltage setting was applied (149 V) with a minimum of 30 runs per measurement, and the Smoluchowski model was used to compute zeta potential from the electrophoretic mobility.

S2.2. Attenuated total reflectance – Fourier transform infrared (ATR-FTIR) spectroscopy

ATR-FTIR spectra were collected from 4000 to 680 cm^{-1} (resolution of 4 cm^{-1}, 100 scans averaged) on a Nicolet iS10 FTIR spectrophotometer equipped with a DTGS KBr detector and OMNI-Sampler accessory and a Ge ATR crystal. The ATR crystal was cleaned with isopropanol and DIW and dried to collect a background spectrum immediately prior to each sample deposition. Then, 5 μL of the PS nanoplastics stock (as purchased without any further processing) was deposited onto the ATR crystal and allowed to dry. The sample spectrum of the dry nanoplastics was processed by subtracting the background spectrum, as well as adding or subtracting water vapor peaks as needed to correct for any differences in water vapor absorbances between the sample and background spectra.

S2.3. Total organic carbon (TOC) analyzer (batch measurement mode)

A portable TOC analyzer (Sievers M9 SEC, Suez, Trevose, PA, USA) was used for both batch and online TOC analysis. 6 M phosphoric acid (Suez, Trevose, PA, USA) was used to acidify the sample for inorganic carbon removal. The oxidizer was prepared using 150 g L^{-1} of ammonium persulfate (98% extra pure, Acros Organics, Fair Lawn, NJ, USA) in phosphate buffer (17 g L^{-1} NaH_2PO_4 and 52.8 g L^{-1} $Na_2HPO_4 \cdot 7H_2O$) with UV activation to oxidize organic carbon to CO_2, which then transfers across a selective permeable membrane and is converted to bicarbonate for detection by conductivity. Both NaH_2PO_4 (anhydrous, ≥ 98%, reagent grade) and $Na_2HPO_4.7H_2O$ (ACS grade) were purchased from VWR Life Science (Solon, OH, USA).

Sample was introduced to the TOC analyzer at 0.5 mL min^{-1}, with acid and oxidizer continuously injected at 2 μL min^{-1} and 4 μL min^{-1}, respectively. For batch analysis, the instrument was flushed with each sample for 10 min, followed by six measurements (2 min each). The mean of the last three measurements was taken. Calibration of the analyzer was verified using potassium hydrogen phthalate (KHP) standards (99.99%, acidimetric standard, ACROS Organics, Fair Lawn, NJ, USA). The batch mode analysis was applied to obtain measured carbon concentrations in the PS nanoplastics, Tween 20, and ESHA, as reported in Section S6.

S2.4. AF4 instrumentation with online TOC analysis

In our instrumental setup, a Wyatt Eclipse AF4 module (Wyatt Technology, Santa Barbara, CA, USA) is attached to an Agilent 1290 Infinity high performance liquid chromatography (HPLC) system (Agilent Technologies, Santa Clara, CA, USA) with a binary pump, degasser, and autosampler. The AF4 short channel (Wyatt Technology) was used with a wide spacer with 250 μm height and a 10 kDa regenerated cellulose (RC) membrane (Ultracel PLCGC, MilliporeSigma, St. Louis, MO, USA) that was die cut in-house. The mobile phase was 0.15 mM Na_2SO_4 (prepared from $Na_2SO_4 \cdot 10H_2O$, 99+%, ACROS Organics, Fair Lawn, NJ, USA). The detector and injection flow rates were set as 0.5 mL min^{-1} and 0.2 mL min^{-1}, respectively. The injection volume was 100 μL. Table S1 presents the optimized AF4 method (see Section S5 for details).

Table S1. AF4 method

Mode	Duration (min)	Cross flow (mL min^{-1})
Elution	6	0.7
Focus	1	2.0
Focus + injection	4	2.0
Elution	58*	0.7
Elution + injection	15	0
Elution	6	0
Elution	10	0.7

*For samples containing clay, the elution time was increased to 88 min instead of 58 min to allow full elution of the particles

The downstream detectors included a UV–Vis diode array detector (DAD, Agilent 1260 Infinity), fluorescence detector (FLD) (Agilent 1260 Infinity), multi-angle light scattering (MALS) detector (Wyatt DAWN HELEOS II, Wyatt Technology) equipped with a dynamic light scattering (DLS) or quasi-elastic light scattering (QELS) detector (Wyatt Technology), differential refractive index (dRI) detector (Optilab T-rEX, Wyatt Technology), and total organic carbon (TOC) detector (Sievers M9-SEC portable TOC analyzer, Suez Water Technologies, Trevose, PA, USA). The order of online detectors after the AF4 channel was UV–Vis, MALS/DLS, FLD, dRI, and TOC, based on the pressure rating of the flow cells and the fact that TOC is a destructive measurement.

The UV absorbance was monitored at 280 nm with the full spectra collected from 190 nm to 600 nm (step 2 nm). The FLD emission and excitation wavelengths were optimized following the instrument manual.[5] Briefly, the Nile Red stained nanoplastics (PS mixtures with 20 mg L^{-1} of each size particle and 10 mg L^{-1} of Nile Red) were injected with AF4 separation, first with a fixed excitation wavelength to identify the value of peak emission wavelength. Initial wavelengths were selected using the fluorescence spectrum reported by Gagné et al.[6] After that, the samples were injected with the identified maximum emission wavelength fixed, and the excitation was scanned to obtain the peak excitation wavelength. The procedure was reiterated on the peak excitation wavelength to identify the maximum emission wavelength. Finally, the photomultiplier tube (PMT) gain was optimized to achieve a higher signal but within the range below detector saturation (< 220 LU). The final optimized emission and excitation wavelengths for the FLD were 620 nm and 230 nm, respectively, and the PMT gain was 15. The FLD spectra were also set to collect in multi-emission mode from 500 to 800 nm at a 10 nm step size. For DLS, a measurement duration of 2 s was used.

The TOC detector was used in online mode (i.e., routing the eluting flow from the AF4 system directly to the TOC analyzer), with turbo mode enabled to collect TOC measurements every 4 s. The acid and oxidizer solutions were the same as described in Section S2.3 and injected at 2 μL min^{-1} and 4 μL min^{-1}, respectively. Data from the TOC detector were directly collected into both the Agilent OpenLab ChemStation and Wyatt ASTRA software (v. 7.3.2.19) during the chromatographic runs. Integrating the TOC data collection with Agilent OpenLab ChemStation required an Agilent 1200 Infinity Universal Interface Box II to receive an analog voltage signal. The Wyatt instruments can receive an analog voltage signal directly; here, the UV and FLD signals were collected through the DAWN HELEOS II and the TOC signal through the Optilab T-rEX. It is noted that the TOC detector outputs an analog current signal (which must be converted to a voltage) and digital MODBUS TCP/IP data. The data resolution of the analog signal was too low to achieve good chromatographic data whenever a wide concentration range was required to fully observe all eluting species. Therefore, a custom digital-analog converter was produced to generate a higher resolution voltage signal using the MODBUS output.[7] A conversion factor of (1.000 Vdc)/(10 mg$_C$ L^{-1}) generally yielded good resolution for the samples here.

For data integration across all detectors (and verification of the system cleanliness and proper functioning of all detectors), bovine serum albumin (BSA, 1 g L^{-1}) was run on the AF4. For BSA separation, the mobile phase was 4 mM phosphate buffer (pH 7) with 25 mM Na_2SO_4. The phosphate buffer composition was 0.23 g L^{-1} KH_2PO_4 (anhydrous ACS grade, Amresco, Solon, OH, USA) and 0.62 g L^{-1} $Na_2HPO_4.7H_2O$. The AF4 method was: (1) elution (1 min); (2) focus (1 min); (3) focus + injection (3 min); (4) focus (2 min); (5) elution (30 min); (6) elution + injection (2 min); and (7) elution (1 min). The cross flow was held constant at 3 mL min^{-1} during all steps. Data were processed using ASTRA software (v. 7.3.2.19, Wyatt Technology). The BSA monomer peak was used as a monodisperse peak for UV, FLD, MALS, and dRI signal alignment and band broadening, as well as an isotropic scatterer for MALS detector normalization. For the TOC analyzer, only alignment was conducted in order to preserve the actual peak widths in order to compare the dispersion or resolution in the TOC to other online detectors.

For particle size analysis, we obtained the radius of gyration (R_g) and hydrodynamic radius (R_h) using the MALS and DLS detectors, respectively, in the ASTRA software. To obtain R_g, the 2^{nd} order Berry model was used, which has previously been shown to have relatively low error for polymeric spheres with sizes of 50 nm, 100 nm, and 500 nm.[8] MALS signals at angles that showed either a low signal to noise ratio, or a saturated signal (typically only observed for the 500 nm nanoplastics) were excluded from analysis. Size data are plotted across the full width at half maximum (FWHM) of the DLS signal. It is further noted that the online DLS detector was moved to position 16 (134°), a higher angle than the default installation (position 12), to achieve better accuracy for particles with radius larger than 75 nm.[9] Additionally, to mitigate contributions of flow artifacts at long timescales in the DLS analysis, we excluded data at decay times $> 4 \times 10^{-3}$ s when processing the autocorrelation function by cumulants analysis.

S3. Batch DLS and ELS characterization of PS nanoplastics and kaolin clay colloids

Batch DLS measurements on the PS nanoplastics and clay are presented in Figure S1a. For complex mixtures comprised of 235 mg L^{-1} of clay with 20 mg L^{-1} of PS nanoplastics (either individually, or a mixture comprised of 20 mg L^{-1} of each size of nanoplastics together, i.e., 80 mg L^{-1} of total nanoplastics), the batch DLS sizes of the mixtures reflect primarily the size of the clay colloids present in higher concentration. Hence, the batch DLS analysis is not able to identify or characterize PS nanoplastics in the presence of the background colloids. The zeta potentials of the four PS nanoplastics and clay were also measured with and without ESHA (concentration of 10 mg_C L^{-1}), as shown in Figure S1b. Measurements were taken in the same background as the AF4 mobile phase (0.15 mM Na_2SO_4). All particles showed a negative zeta potential, with more strongly negative zeta potentials observed after the addition of ESHA, suggesting adsorption of the negatively charged ESHA to all particles (PS and clay). The origin of the negative surface charge on the PS nanoplastics as purchased (without ESHA) is not apparent, given that pristine PS as well as the Tween 20 surfactant used in the PS stock are both expected to be nonionic. The zeta potentials of the PS nanoplastics were also measured in an approximately equivalent ionic strength of 0.5 mM sodium nitrate ($NaNO_3$) (Thermo Fisher Scientific, Fair Lawn, NJ, USA) as opposed to 0.15 mM Na_2SO_4 and similarly showed negative charges, indicating that SO_4^{2-} adsorption from the background solution is not responsible for the negative charge.

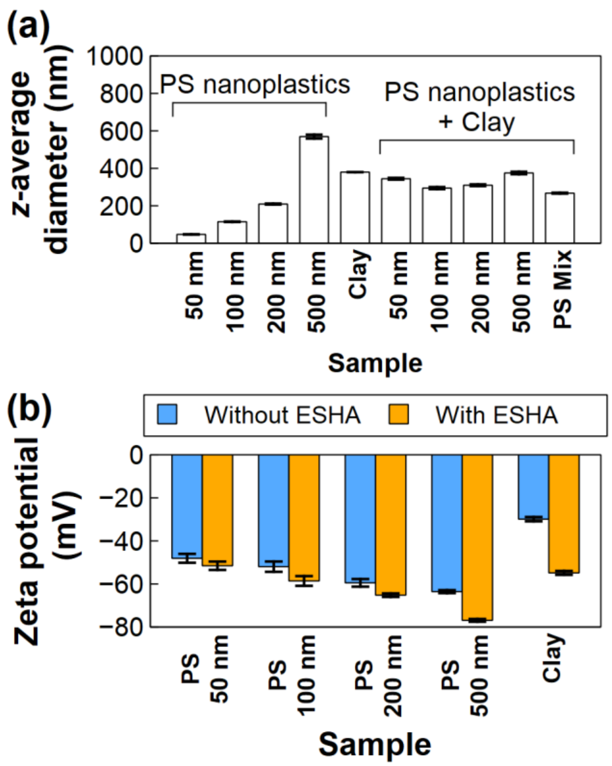

Figure S1. Batch *z*-average diameters of individual PS nanoplastics, the clay colloid stock, individual PS nanoplastics with clay, and the mixture of the four PS nanoplastic sizes with clay (a), and zeta potentials of the individual PS nanoplastics and clay without and with ESHA (b). All PS samples were prepared with 20 mg L^{-1} of each nanoplastics size and/or 235 mg L^{-1} of clay in 0.15 mM Na_2SO_4 (i.e., matching the AF4 conditions), except the size of the clay stock was measured as collected at 570 mg L^{-1} in deionized water. Error bars represent the standard deviation of five measurement replicates.

S4. ATR-FTIR analysis of PS nanoplastics

ATR-FTIR spectra for the PS nanoplastics stocks are provided in Figure S2. All samples show the expected FTIR absorbance peaks for PS at 698 and 757 cm^{-1} (C–H out-of-plane bending vibration of the aromatic ring), 1452 cm^{-1} (C–H deformation of CH_2), 1493 cm^{-1} (C–H stretching vibration of ring in plane), 1602 cm^{-1} (C–C stretching frequency of ring in plane), 2851 cm^{-1} (C–H symmetrical stretching vibration of CH_2), 2923 (C–H asymmetrical stretching vibration of CH_2), and 3025, 3060, and 3082 cm^{-1} (C–H aromatic stretching vibration). All PS peak assignments are those reported by Bhutto et al.[10] Additional peaks at 1120 cm^{-1} and 2038 cm^{-1} are observed in the 50 nm and 500 nm PS stocks; the 1120 cm^{-1} peak may be attributable to C–O in the Tween 20 surfactant. The weak absorbance at > 3100 cm^{-1} may also be attributed to O–H in Tween 20. It is noted that the 200 nm PS (which resisted uptake of Nile Red) shows absorbances at 1697 cm^{-1} (typically attributed to C=O groups) and 1220 cm^{-1} that are not observed in the other PS stocks.

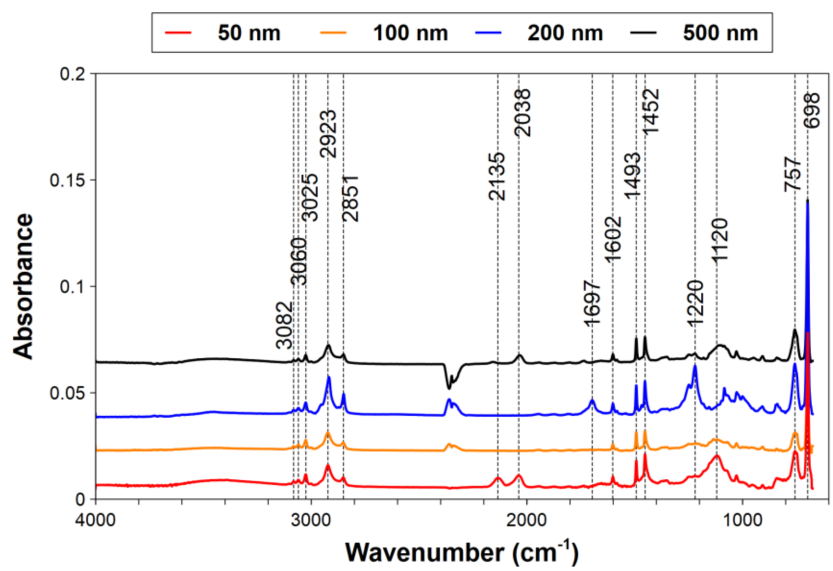

Figure S2. ATR-FTIR spectra of the four PS nanoplastics from the stocks as purchased (5 μL deposited from stock suspensions of nominal 10 g L^{-1} of PS with 1 g L^{-1} of Tween 20 surfactant). All spectra are presented at a common scale but staggered for clarity of visualization.

S5. Optimization of AF4 cross flow for nanoplastics separations

The AF4 cross flow was first optimized for size separation of the four sizes of nanoplastics (50 nm, 100 nm, 200 nm, and 500 nm) using an AF4 channel height of 250 μm and 10 kDa regenerated cellulose ultrafiltration membrane as the accumulation wall. The nanoplastics were diluted in deionized water from the purchased stocks at nominal concentrations of 20 mg L^{-1} of each of the four sizes. The flow was fixed at 2 mL min^{-1} for 4 min, and constant cross flows ranging from 0.3 mL min^{-1} to 1.0 mL min^{-1} were evaluated (Figure S3). It is noted that polyvinyl alcohol (PVA) was injected as a surfactant that could potentially reduce AF4 membrane fouling (i.e., improve nanoparticle recovery) in prior injections before analyzing the PS mixtures. Residual PVA in the system was released as a void peak at the beginning of each run; although the PVA does not show a UV absorbance (Figure S3a), the TOC detector was sensitive to PVA in the void peak (Figure S3b, peak labeled with an asterisk). Separation of the smallest (50 nm) nanoplastics from this void peak was also considered in selecting the optimal cross flow. (For all subsequent experiments, no surfactant was introduced so that no void peak is observed in the PS nanoplastics except when intentionally adding humic acids to the sample).

Increasing the cross flow from 0.3 mL min^{-1} to 0.85 mL min^{-1} resulted in better separation of peak elution times for the four particle sizes, and especially better separation of the 50 nm nanoplastics from the void peak. However, higher cross flow also resulted in more extensive peak broadening, and increasing cross flow further to 1.0 mL min^{-1} resulted in a substantial overlap of the 200 nm and 500 nm peaks. Gradient elution has previously been recommended for polydisperse nanoplastics analysis by AF4.[11] Here, a method was tested starting with 1.0 mL min^{-1} constant cross flow held for 20 min to separate the void, 50 nm, and 100 nm peaks, followed by an exponential cross flow decay to 0.5 mL min^{-1} over the next 38 min), but poor separation of the 200 nm and 500 nm nanoplastics was observed. Hence, 0.7 mL min^{-1} was selected as the optimal cross flow for providing the most distinct separation of the void peak and each size of nanoplastics.

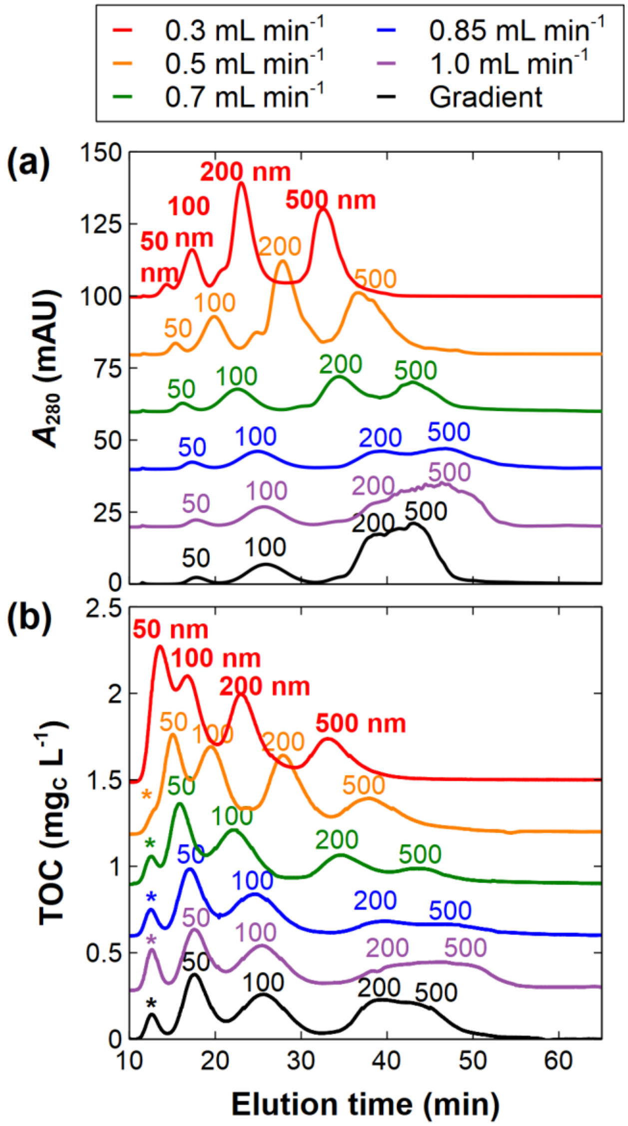

Figure S3. Cross flow optimization for AF4 separation of PS nanoplastics mixtures (50 nm, 100 nm, 200 nm, and 500 nm, each at a nominal concentration of 20 mg L^{-1}) with UV (a) and TOC (b) detection. The asterisk (*) denotes residual polyvinyl alcohol surfactant introduced prior to the analyses that elutes as a void peak immediately after releasing the focus flow and initiating the elution step. All chromatograms are presented at a common scale but staggered (i.e., baseline shifted) for clarity of visualization.

S6. Quantification of PS nanoplastics by gravimetric and TOC analysis

To thoroughly evaluate the capability of the TOC analyzer to quantify the mass concentration of PS nanoplastics, a series of measurements were compared to evaluate both the concentration of the stocks as purchased as well as to quantify losses in efficiency or recovery of the PS nanoplastics in all stages of the measurement (oxidation in the TOC analyzer, losses in the overall AF4 system such as the injection loop and tubing, and losses during AF4 separation). The measurements are summarized in Figure S4 and discussed in detail hereafter.

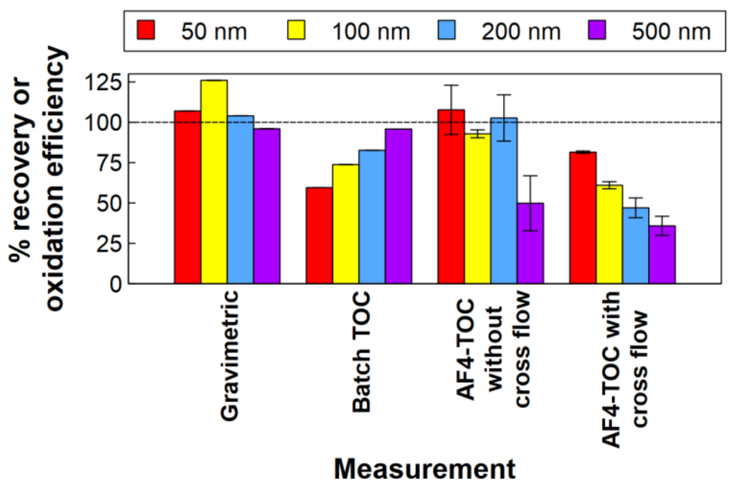

Figure S4. Recovery or oxidation efficiency of the four sizes of PS nanoplastics. Gravimetric measurements represent % mass measured relative to the nominal (expected) mass after lyophilization of the as-purchased PS stock suspensions, batch TOC measurements represent the oxidation efficiency (after correcting for the gravimetric results), AF4-TOC without cross flow represents the % recovery of individual sizes of nanoplastics injected to the AF4 system without separation, and AF4-TOC with cross flow represents the % recovery of nanoplastics from a mixture of all four sizes with separation applied. The expected contribution of Tween 20 surfactant in the stocks was subtracted from all measurements except AF4-TOC with cross flow (where *in situ* purification is achieved). Error bars on the AF4-TOC measurements represent the standard deviation across triplicate AF4 runs.

Gravimetric measurements were conducted on each size of PS nanoplastics (50 nm, 100 nm, 200 nm, and 500 nm) to verify the total mass concentrations of nonvolatile material after lyophilization of 1 mL of each stock (method described in Section S1.1). The concentration of Tween 20 was assumed to be exact (i.e., 0.1 wt % or 1 g L^{-1} as reported), and the expected mass of Tween 20 ($m_{\text{Tween 20}}$) was hence subtracted from the total measured mass (m_{meausred}) to determine the PS mass "recovery" relative to the nominal PS mass ($m_{\text{nominal,PS}}$), as in Equation S1 for 1 mL of stock:

$$\text{PS mass recovery} = \frac{m_{\text{measured}} - m_{\text{Tween 20}}}{m_{\text{nominal,PS}}} = \frac{m_{\text{measured}} - 1\ \text{mg}}{10\ \text{mg}} \tag{S1}$$

The mass recovery from this analysis (Figure S4, "Gravimetric") could then be used to adjust nominal mass concentrations to "true" mass concentrations of PS.

Batch TOC measurements were then collected on the four individual PS stocks to evaluate the oxidation efficiency of the nanoplastics without having to consider issues of incomplete recovery from the AF4 system. The as-purchased stocks were diluted in deionized water to a nominal concentration of 5 mg L^{-1} PS with 0.5 mg L^{-1} Tween 20 surfactant (based on the reported manufacturer stock concentration of 1 wt % or 10 g L^{-1} PS). Expected mass concentrations, *C*, were converted to concentrations as carbon using the wt % carbon from the chemical formulas for Tween 20 or PS. The Tween 20 contribution to the TOC measurement ($TOC_{\text{Tween 20}}$) was subtracted from the total measured TOC concentration (TOC_{measured}), with the oxidation efficiency in the TOC analyzer measured independently as 92.4% by batch TOC analysis of a known Tween 20 concentration diluted in deionized water to 10 mg_C L^{-1} from pure Tween 20 stock. After correcting the nominal concentrations to the "true" PS concentrations and accounting for the known wt % carbon in polystyrene (92.3 wt % C), the oxidation efficiencies for each size of PS nanoplastics were computed (Equation S2):

$$\text{PS oxidation efficiency} = \frac{TOC_{\text{measured}} - TOC_{\text{Tween 20}}}{C_{\text{nominal,PS}}\ (\%\ \text{C})_{\text{PS}}\ (\text{Mass recovery})_{\text{PS,gravimetric}}}$$

$$= \frac{TOC_{\text{measured}} - C_{\text{Tween 20}}\ (\%\ \text{C})_{\text{Tween 20}}\ (\text{Oxidation efficiency})_{\text{Tween 20}}}{C_{\text{nominal,PS}}\ (\%\ \text{C})_{\text{PS}}\ (\text{Mass recovery})_{\text{PS,gravimetric}}}$$

$$= \frac{TOC_{\text{measured}} - (0.5\ \text{mg L}^{-1}\ \text{Tween 20})\left(0.567\ \frac{\text{g C}}{\text{g Tween 20}}\right)\left(0.924\ \frac{\text{g C oxidized}}{\text{g C in Tween 20}}\right)}{(5\ \text{mg L}^{-1}\ \text{nominal PS})\left(0.923\ \frac{\text{g C}}{\text{g PS}}\right)(\text{Mass recovery})_{\text{PS,gravimetric}}} \quad \text{(S2)}$$

After gravimetric correction, the results (Figure S4, "Batch TOC") suggest that oxidation efficiency in the TOC analyzer declines as particle size decreases. The reason for this observed trend is not evident, considering that the smaller nanoplastics have higher surface area to volume exposed for reaction with the persulfate oxidant in the TOC analysis. In addition, the PS particle density is not expected to vary with size,[12] although there may be a variable surfactant density profile in the particles.[13] In any case, these results suggest that oxidation efficiency should be considered to accurately interpret the quantitative TOC measurements.

The TOC was then evaluated in online mode, first for injections of each of the four individual sizes of PS nanoplastics into the completely assembled AF4 system (i.e., with the AF4 channel online) with no focus or cross flow applied for separation (Figure S4, "AF4-TOC without cross flow"). Samples were injected at nominal concentrations of 20 mg L^{-1} PS with 2 mg L^{-1} Tween 20 surfactant. The total mass of C measured in the unseparated sample ($m_{\text{C,measured}}$) was determined by multiplying the peak area by the flow rate. Corrections were again made to subtract the Tween 20 contribution ($m_{\text{C,Tween 20}}$) and to adjust the nominal mass of PS ($m_{\text{nominal,PS}}$) for both the "true" PS concentration and the oxidation efficiency measured in the gravimetric and batch TOC measurements, respectively (Equation S3):

$$\text{PS recovery} = \frac{m_{\text{C,measured}} - m_{\text{C,Tween 20}}}{m_{\text{nominal,PS}}\ (\%\ \text{C})_{\text{PS}}\ (\text{Mass recovery})_{\text{PS,gravimetric}}\ (\text{Oxidation efficiency})_{\text{PS}}} \quad \text{(S3)}$$

Nearly 100% recovery was achieved for the 50 nm, 100 nm, and 200 nm nanoplastics, validating the TOC measurements in the online mode. Lower recovery for the 500 nm nanoplastics likely represents fouling of the AF4 system rather than incomplete oxidation in the TOC analyzer, as recovery was initially high (80 %) but declined with subsequent injections.

Finally, TOC recovery was evaluated in the AF4-TOC analysis on mixtures of nominal 20 mg L^{-1} of each size of PS nanoplastics with 0.7 mL min^{-1} cross flow applied for size separation (Figure S4, "AF4-TOC with cross flow"). Because the Tween 20 surfactant is removed through the ultrafiltration membrane in the AF4 channel during sample focusing, Equation S3 was applied without the Tween 20 subtraction to compute recovery. Declining recovery was observed with increasing particle size. Given that the online TOC measurements were largely validated in the prior analysis without cross flow, incomplete recovery is attributed to loss onto the AF4 membrane during the focus or elution stages, with larger particles that reside nearer to the membrane showing higher losses. It is noted that for clarity of analysis, the calibration curves in Section S9 (measured across four PS concentrations) are reported for the peak areas directly as collected, without applying corrections for the gravimetric analysis or oxidation efficiency.

S7. LS and dRI detector signals for AF4 calibration runs on PS nanoplastic mixtures

In addition to the UV and TOC detectors coupled to the AF4 (shown in Figure 1), light scattering and dRI detectors were also included online. AF4 chromatograms for the light scattering signal at the 90 ° detector (LS11) and dRI detector are provided in Figure S5.

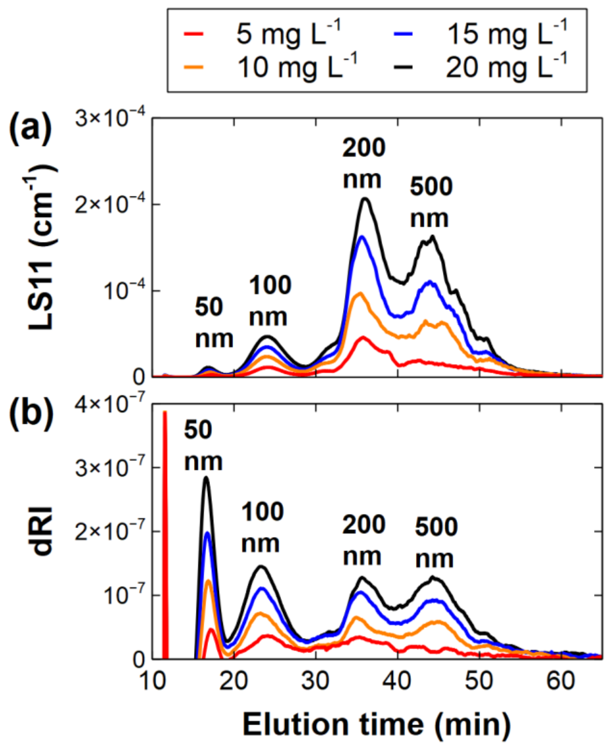

Figure S5. AF4 chromatograms for the LS11 detector (a) and dRI detector (b) for the same calibration samples presented in Figure 1, where the LS11 value is the Rayleigh ratio (a measure of the scattered light intensity relative to the incident intensity) measured at 90° scattering angle.

S8. Elution times and computed resolution for PS nanoplastics in AF4-UV and AF4-TOC

The peak elution times and computed peak resolution are presented in Figure S6 for triplicate runs on the mixtures of PS nanoplastics at various concentrations (representative chromatograms in Figures 1 and S5).

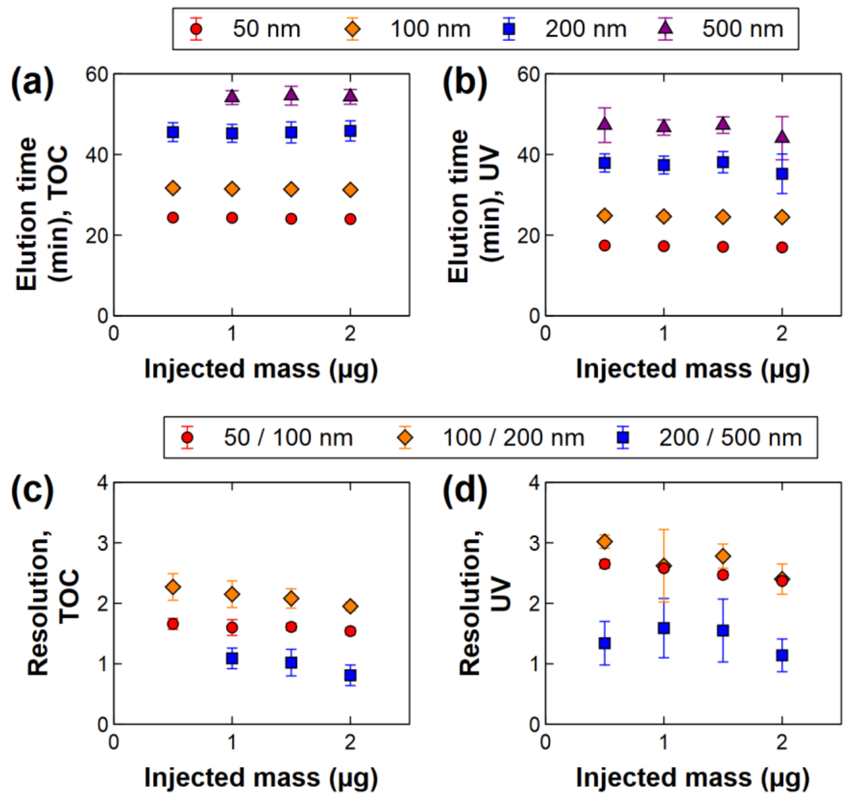

Figure S6. Elution times for AF4-TOC (a) and AF4-UV (b) analysis of mixtures of 50 nm, 100 nm, 200 nm, and 500 nm PS nanoplastics, and resolution computed for adjacent eluting peaks for AF4-TOC (c) and AF4-UV (d) analysis. Representative AF4 chromatograms are shown in Figures 1 and S5. Elution times could not be determined for the lowest concentration of 500 nm particles in the TOC analysis because of the peak broadening and overlap with the 200 nm peak. Error bars represent the standard deviation across triplicate AF4 runs.

The resolution between adjacent peaks was computed using Equation S4,[14]

$$\text{Resolution} = \frac{\Delta t_R}{\langle w_{\text{FWHM}} \rangle} \quad \text{(S4)}$$

where Δt_R is the difference in peak retention times and $\langle w_{FWHM} \rangle$ is the mean of the full width at half-maximum (FWHM) of the two eluting peaks. It is noted that although a resolution > 1.5 represents baseline resolution for Gaussian peaks, here "baseline" resolution values were computed for cases that do not visually show baseline resolution, which is attributed to the non-Gaussian peak shapes. Resolution is generally lower for the TOC detector because of the high dispersion due to mixing with the acid and oxidizer reagents and the large volume between sample introduction to the TOC analyzer, oxidation of the organic carbon to CO_2, and detection of the CO_2 generated. However, separation of each of the four sizes of nanoplastics is still largely evident in the chromatograms, except for the 200 nm and 500 nm peaks at the lowest injected mass (Figure 1b).

S9. Calibration curves for AF4 analyses and limit of quantitation for AF4-TOC

Calibration curves were developed using peak areas from triplicate AF4 analyses on mixtures of the four PS nanoplastics sizes at nominal concentrations of (5, 10, 15, and 20) mg L^{-1} of PS, i.e., injected masses of (0.5, 1.0, 1.5, and 2.0) μg for a 100 μL injection volume. Representative chromatograms are shown in Figures 1 and S5. The TOC, UV_{280}, and dRI calibration curves are presented as the raw measurements in Figure S7 and generally show a linear response of each detector to each size of nanoplastics.

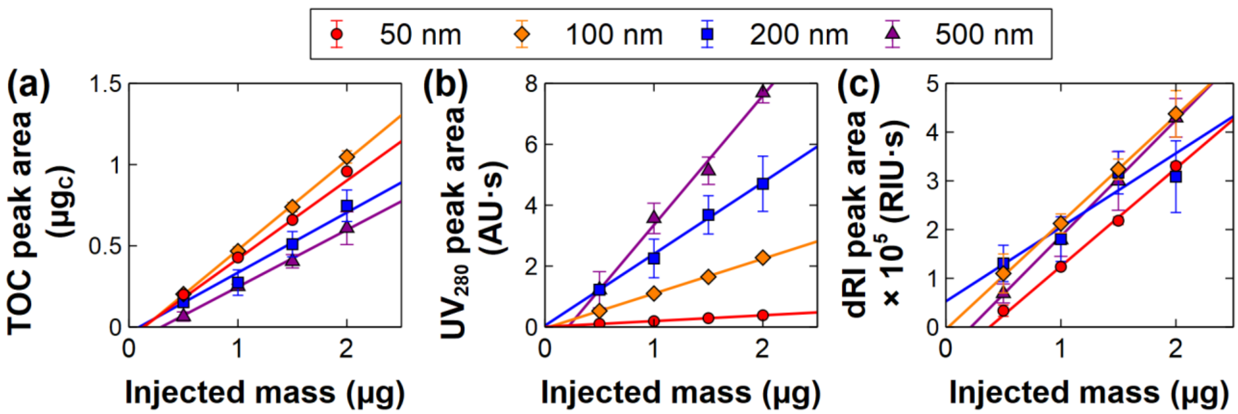

Figure S7. Calibration curves for AF4 with online TOC (a), UV_{280} (b), and dRI (c) detection, as evaluated using peak areas from AF4 chromatograms on mixtures of 50 nm, 100 nm, 200 nm, and 500 nm PS nanoplastics (representative chromatograms in Figures 1 and S5). TOC signal peak areas in V·s were converted to μg_C using the analog conversion factor (1.000 V = 10 mg_C L^{-1}) and the detector flow rate (0.5 mL min^{-1}). Error bars represent the standard deviation across triplicate AF4 runs.

The limit of quantitation (LOQ) for each PS nanoplastics size in the AF4-TOC analysis was estimated based on the signal-to-noise ratio of the peak height to the standard deviation, σ, in the baseline noise in the TOC detector signal (e.g. $\sigma = 3.52 \times 10^{-5}$ V, as measured over 6 min of baseline data collection at the beginning of a representative sample run). Calibration curves based on TOC peak heights are presented in Figure S8. The LOQ was estimated by extrapolating the calibration curves in Figure S8 to the injected mass corresponding to a peak height of 10σ for each size of PS nanoplastics, as reported in Table S2. Note that given the generally low baseline noise, the LOQ is determined largely by the non-zero intercept representing loss of nanoplastics (i.e., incomplete recovery) during the AF4 separation, rather than the baseline noise.

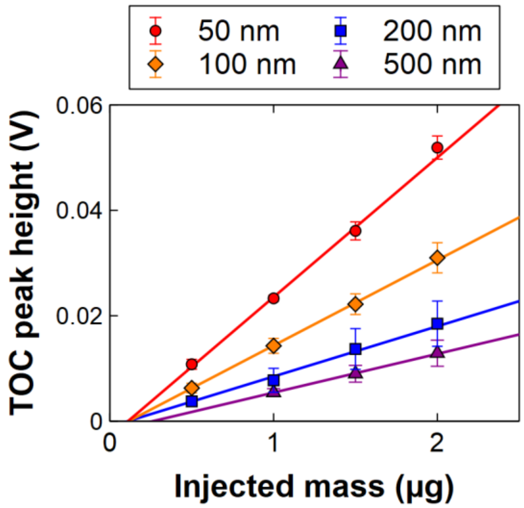

Figure S8. TOC peak heights for AF4 with online TOC detection, as evaluated on AF4 chromatograms on mixtures of 50 nm, 100 nm, 200 nm, and 500 nm PS nanoplastics (representative chromatograms in Figures 1 and S5). A peak height could not be determined for the lowest concentration of 500 nm particles because of the overlap with the 200 nm peak. Error bars represent the standard deviation across triplicate AF4 runs.

Table S2. Limits of quantitation for PS nanoplastics in AF4-TOC analysis

PS Nanoplastic Diameter	LOQ (μg)†
50 nm	0.14 ± 0.01
100 nm	0.15 ± 0.02
200 nm	0.20 ± 0.04
500 nm	0.28 ± 0.07

†Results are reported as the mean ± standard deviation of triplicate calibration sets.

S9. AF4 analysis of clay and ESHA with individual 200 nm and 500 nm PS nanoplastics

To confirm lack of sensitivity of the TOC detector to the inorganic clay colloids, a mixture of clay and ESHA was injected for analysis without nanoplastics (Figure S9). In addition, to better identify the peaks observed by AF4-TOC on the PS mixture of all four sizes with the clay and ESHA, individual PS sizes of 200 nm and 500 nm (where the clay coelutes) were mixed with clay and ESHA and analyzed by AF4 to separately identify their elution times (Figure S9).

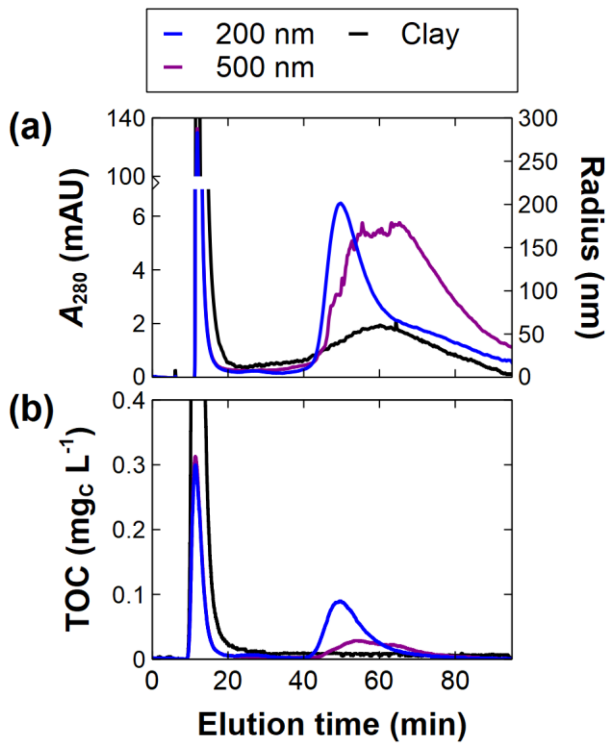

Figure S9. AF4-UV (a) and AF4-TOC (b) chromatograms for a mixture of 235 mg L^{-1} of clay and 10 mg L^{-1} of ESHA (black), and individual 200 nm and 500 nm PS nanoplastics spiked at 20 mg L^{-1} into the clay and ESHA mixture. Note the clay-ESHA mixture alone showed a low signal overall (likely due to membrane fouling) and is scaled by a factor of 5 relative to the other chromatograms for better visualization.

S10. Influence of clay concentration on AF4 separations and nanoplastics detection

The collected concentration of kaolin clay colloids was 570 mg L^{-1} in the supernatant of a 1 g L^{-1} clay stock suspension after probe sonication followed by centrifugation, as described in Section S1.3. In preliminary measurements, the clay was spiked at the as-collected concentration with the four sizes of PS nanoplastics (at nominal 20 mg L^{-1} of each size) and ESHA (at 10 mg_C L^{-1}). Despite the larger size of the clay colloids (≈ 300 to 400 nm, Figure S1a), the clay co-eluted over both the 100 nm and 200 nm nanoplastics (Figure S10a) when injected at 570 mg L^{-1}, as observed by comparing the UV signal (which is sensitive to scattering from the clay particles) to the TOC signal (selective for only the PS nanoplastics). However, larger particles would be expected to elute later than smaller particles in normal AF4 mode.

Overloading of sample has previously been reported to result in more rapid elution than expected.[15] Hence, a dilution of the clay to 235 mg L^{-1} (also spiked with 20 mg L^{-1} of each of the four nanoplastics and 10 mg_C L^{-1} of ESHA) was evaluated (Figure S10b). Reducing the clay concentration resulted in successful separation of the UV signal of the 100 nm nanoplastics from that of the clay. These results indicate that sample concentration and overloading effects can be important to consider, particularly for UV or other detection modes that are sensitive to interference from species such as natural inorganic colloids if they coelute with the nanoplastics. However, the TOC detection of the nanoplastics was notably insensitive to the clay particles regardless of whether overloading occurred (Figure S10), and hence can provide a more robust evaluation of the nanoplastics concentration as well as the size of the two smaller nanoplastics (50 nm and 100 nm) based on their elution time. It is again noted that fouling of the AF4 membrane by the clay colloids resulted in poor distinction and/or diminished recovery of the 200 nm and 500 nm PS nanoplastics. This issue is a limitation of the AF4 separation rather than the detectors, but is most straightforward to assess using the TOC detector to selectively probe for the nanoplastics distinctly from any coeluting clay colloids.

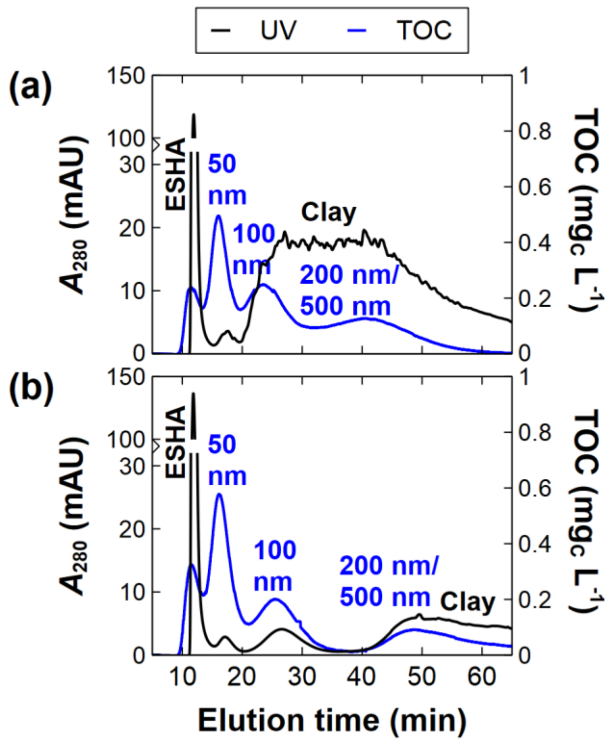

Figure S10. AF4-UV and AF4-TOC chromatograms for complex mixtures of PS nanoplastics (nominal 20 mg L^{-1} each of 50 nm, 100 nm, 200 nm, and 500 nm), ESHA (10 mg_C L^{-1}), and clay colloids at 570 mg L^{-1} (a) or 235 mg L^{-1} (b). A reliable light scattering analysis could not be achieved on the nanoplastics in (a) because of the coelution of the clay; R_g and R_h for (b) are shown in Figure 3.

S11. AF4 analysis of PS nanoplastics in complex matrices after staining with Nile Red

AF4 chromatograms are presented in Figure S11 for mixtures of the four sizes of PS nanoplastics with ESHA and clay colloids.

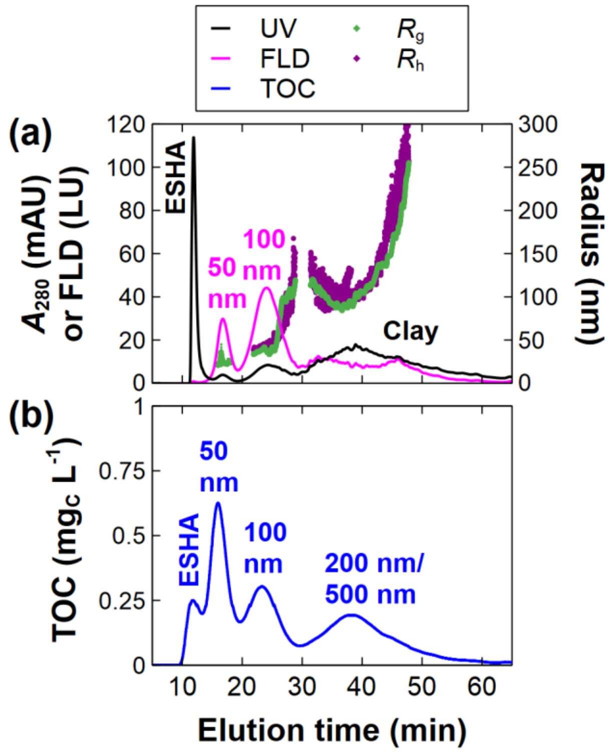

Figure S11. AF4-UV and AF4-FLD (a) and AF4-TOC (b) chromatograms for complex mixtures of PS nanoplastics (nominal 20 mg L^{-1} each of 50 nm, 100 nm, 200 nm, and 500 nm), ESHA (10 mg_C L^{-1}), and clay colloids at 235 mg L^{-1} after staining with 10 mg L^{-1} of Nile Red. The R_g and R_h analysis by MALS and DLS, respectively, are provided in (a).

The Nile Red staining provides selective detection of the 50 nm and 100 nm nanoplastics (Figure S11a) relative to the ESHA and clay colloids. However, low uptake of Nile Red by the 200 nm nanoplastics (as verified on AF4-FLD measurements on individually stained and injected nanoplastics of each size, as well as mixtures of the nanoplastics in Figure 2) resulted in poor capability to detect the 200 nm nanoplastics. In contrast, TOC analysis provides more robust detection of all nanoplastics in the mixture, although peak overlap of the ESHA and the 50 nm PS nanoplastics was observed (Figure S11b). The results suggest that AF4-TOC detection and Nile Red staining for AF4-FLD could potentially be utilized as complementary approaches to distinguish dissolved organic matter from nanoplastics.

References

1. B. C. Suedel and J. H. Rodgers Jr, *Environ. Toxicol. Chem.*, 1994, **13**, 1163-1175.
2. B. C. Suedel and J. H. Rodgers Jr, *Environ. Toxicol. Chem.*, 1994, **13**, 1639-1648.
3. M. C. Eimers, R. Douglas Evans and P. M. Welbourn, *Chemosphere*, 2002, **46**, 543-551.
4. H. El Hadri, S. M. Louie and V. A. Hackley, *Environ. Sci.: Nano*, 2018, **5**, 203-214.
5. Agilent Technologies, *Agilent 1260 Infinity Fluorescence Detector: User Manual*, Waldbronn, Germany, 2013.
6. F. Gagné, J. Auclair and B. Quinn, *Environ. Sci. Pollut. Res.*, 2019, **26**, 33524-33531.
7. H. W. Louie and S. M. Louie, Texas Data Repository, 2021, https://doi.org/10.18738/T8/LZNHUX.
8. M. Andersson, B. Wittgren and K.-G. Wahlund, *Anal. Chem.*, 2003, **75**, 4279-4291.
9. J. Parot, F. Caputo, D. Mehn, V. A. Hackley and L. Calzolai, *J. Controlled Release*, 2020, **320**, 495-510.
10. A. A. Bhutto, D. Vesely and B. J. Gabrys, *Polymer*, 2003, **44**, 6627-6631.
11. J. Gigault, H. El Hadri, S. Reynaud, E. Deniau and B. Grassl, *Anal. Bioanal. Chem.*, 2017, **409**, 6761-6769.
12. M. Godin, A. K. Bryan, T. P. Burg, K. Babcock and S. R. Manalis, *Appl. Phys. Lett.*, 2007, **91**, 123121.
13. A. E. Chalykh, V. K. Gerasimov, U. V. Nikulova, A. A. Ezhova and I. A. Gritskova, *Russ. Chem. Bull.*, 2019, **68**, 1735-1740.
14. British Standards Institution, *PD ISO/TS 21362:2018: Nanotechnologies — Analysis of nano-objects using asymmetrical-flow and centrifugal field-flow fractionation*, 2018.
15. M. E. Schimpf, K. Caldwell and J. C. Giddings, eds., *Field-Flow Fractionation Handbook*, John Wiley & Sons, Inc., New York, NY, USA, 2000.